Environmentally safe ZVI/ZnS-based polymer composite for lindane degradation in water: Assessment of photocatalytic activity and eco-toxicity

Environmentally safe ZVI/ZnS-based polymer composite for lindane degradation in water: assessment of photocatalytic activity and eco-toxicity

Raffaella Rescigno[1], Olga Sacco[1*], Stefania Pragliola[1], Luisa Albarano[2], Giovanni Libralato[2], Giusy Lofrano[3*], Vincenzo Romano Spica[3], Olimpia Tammaro[4], Giorgia Montalbano[4], Serena Esposito[4] Vincenzo Vaiano[5] and VincenzoVenditto[1]

[1]Department of Chemistry and Biology "A. Zambelli", INSTM research unit, University of Salerno, via Giovanni Paolo II, 132, 84084 Fisciano (Salerno), Italy

[2]Department of Biology, University of Naples Federico II, Monte Sant'Angelo University Complex - Building 7, Via Vicinale Cupa Cintia 26, 80126, Naples, Italy

[3]Department of Movement, Human and Health Sciences, University of Rome Foro Italico, Piazza Lauro De Bosis, 15, 00135 Roma, Italy

[4]Department of Applied Science and Technology and INSTM Unit of Torino – Politecnico, Politecnico di Torino, Corso Duca degli Abruzzi 24, 10129, Torino, Italy.

[5]Department of Industrial Engineering, INSTM research unit, University of Salerno, via Giovanni Paolo II, 132, 84084 Fisciano (Salerno), Italy

*Corresponding authors: Olga Sacco (osacco@unisa.it); Giusy Lofrano (giusy.lofrano@uniroma4.it)

Abstract

Monolithic composite aerogel based on a photocatalytic system, constituted by Fe^0 (ZVI) coupled with ZnS (FZ), embedded into syndiotactic polystyrene (sPS) matrix was used, for the first time, in the lindane degradation under UV light. The content of FZ photocatalyst inside the monolithic composite aerogel (FZsPS) composite was 3 wt%. FESEM images of FZsPS indicate that the FZ photocatalyst is well dispersed in the polymer matrix. EDS analyses and temperature-programmed reduction (TPR-H_2) measurements revealed an interpenetrated structure of the ZVI and ZnS phases as well the presence of some iron in an oxidized form. Photocatalytic activity data showed that in presence FZsPS aerogel, the almost complete lindane degradation was achieved after only 30 min of UV irradiation time. FZsPS was also effective in the lindane mineralization since a TOC removal of about 94% was detected after 180 min of treatment time. Remarkably, based on the toxicity evaluation on *Artemia franciscana*, while the bare FZ photocatalyst showed significant toxicity per se, no toxicity or genotoxicity was found in the water treated with the FZsPS composite system where FZ is immobilized into the sPS aerogel matrix. Therefore the proposed composite photocatalyst can be considered as a model for a strategy to eliminate the environmental impact of catalysts that would otherwise be harmful to water.

Keywords: ZVI/ZnS polymer composite; polymeric aerogel; lindane; photocatalytic degradation; toxic and genotoxic effects

1. Introduction

Lindane is the common name of the γ-isomer of hexachlorocyclohexane (HCH), an organochlorine pesticide (OCP) widely used from 1950s to 1980s for both agricultural and non-agricultural purposes (USEPA, 2006 [1]). It has been used for example on fruits and vegetables, to control insects and pests, but also for seed and soil treatment, for the treatment of trees and wood, especially in coniferous forests and for the treatment against ectoparasites in both veterinary and human applications [2-4]. Its global production was around 600,000 tonnes during the period from 1950s to 2000s [5]. Italy was one of the top 10 countries with the highest usage of Europe [6].

The persistence of lindane in aquatic environments has been widely documented, as well as its toxicity to aquatic organisms [7]. The (L(E)C50) and chronic (NOEC) toxicity values are at the level of µg/L for several type of fishes and aquatic invertebrates. Several concerns have been reported regarding human health. AMAP reported an increase in HCH isomers in human tissues and breast milk [8]. It has been identified as a potential endocrine-disrupting chemical [9]. The United States Environmental Protection Agency (US EPA) and the World Health Organization (WHO) classify lindane as a potent carcinogen and teratogen agent [10, 11]. The International Agency for Research on Cancer (IARC) has associated its exposure with one of the causes of non-Hodgkin's lymphoma (NHL) (IARC, 2016).

For these reasons, lindane was listed within the persistent organic pollutants by the 2009 Stockholm Convention [12]. As a result, its production and agricultural use were banned in more than 50 countries worldwide by 2010 [5], but pharmaceutical use is permitted as a second-line treatment for scabies and lice [13]. Therefore, HCH concentrations have been detected in water bodies all over the world (ranging from

0.087 to 5509 µg/L), as well as in drinking water, also due to its strong refractory degradation [14], becoming a concern of global relevance.

Traditional methods require long treatment times for lindane degradation because it is a hydrophobic organic molecule (logKow >3.5) [15, 16]. Thus, much effort is being made in developing more efficient and sustainable technologies to remove lindane from water.

Among several processes allowing the breaking of the C-Cl bond, technologies based on zero-valent iron (ZVI), which reacts with halogenated organic pollutants (RX) acting as a very powerful reducing agent [17], result as the most promising. In recent decades, the use zero-valent iron (ZVI) has been proposed for depolluting soils and aquifers because ZVI is highly reactive and inexpensive [18, 19]. However, the halogenated organic pollutants degradation rates in presence of ZVI decrease over time [20] because Fe^0 is easily oxidized to Fe^{2+} [21] according to the following general reaction [21-24]:

$Fe^0 + RX + H^+ = Fe^{2+} + RH + X^-$.

On the other hand, advanced oxidation processes (AOPs), such as heterogeneous photocatalysis, can degrade organic pollutants into harmless end products, including lindane [13, 25-28], but the degradation performance is generally low when photocatalysis is used for the treatment of water polluted by chlorinated organic compounds (such as perchloroethylene and lindane) [26, 29-33]. Indeed, in the case of lindane, it is reported that treatment times higher than 2 h are required for the almost complete pollutant degradation. Hence to improve the efficiency of photocatalytic processes for the degradation of halogenated organic pollutants, some authors have proposed to couple semiconductor photocatalysts, such as TiO_2, ZnO, g−C_3N_4 and g−C_3N_4/MoS_2, with ZVI to simultaneously exploit the photocatalytic

degradation properties with the reductive action of ZVI [34-38]. In this perspective, Sacco et al. selected ZnS as a suitable semiconductor to be coupled with ZVI and demonstrated as it is possible to obtain a powder composite capable of degrading chlorobenzene more efficiently than ZnS and ZVI alone, evidencing that the simultaneous presence of UV light and ZnS avoid the ZVI oxidative corrosion phenomena, also preserving a high reactivity after several reuse cycles [39]. However, despite the interesting degradation performances reported by such photocatalytic composites, it must be considered that they have been used in slurry photoreactors in which the catalytic powders are dispersed within the aqueous medium. Therefore, the need for a post-treatment step for the separation of catalysts from the treated water remains the main constraint to the full-scale application of photocatalytic systems [40-43]. Moreover, the use of suspended particles for wastewater treatment implies their possible release into the environment, inducing a health risk due to the possible toxicity of these nanoparticles [44-49].

To overcome these drawbacks, the catalytic materials could be immobilized on the surface of suitable macroscopic supports [50, 51] or dispersed within the porous structure of supports having a high affinity towards the target pollutant [52, 53].

To date, among the different supports for photocatalysts (such as glass, ceramic or zeolites [54-56]) polymers are attracting more and more attention in the literature concerning heterogeneous photocatalysis [57-60].

Recent research papers reported that monolithic syndiotactic polystyrene (sPS) aerogels are promising supports for photocatalytic applications due to their good mechanical properties and the nanoporous crystalline phase which confers high surface areas and good sorption properties [59, 61-66].

This research aimed at investigating for the first time the behavior of a composite aerogel (FZsPS) based on sPS and Fe^0/ZnS, in the photocatalytic degradation of lindane. The kinetic of degradation was fully characterized from a chemical and ecotoxicological viewpoint. In particular, embryo-larval and adult-related effects on *Artemia franciscana* were evaluated. Genotoxicity testing was also performed to determine potential hazards for direct or indirect DNA interaction.

It is worthwhile to note that to date no scientific paper reports toxicological results on the treated water coming from the photocatalytic degradation of lindane by using composite aerogels.

2. Materials and methods

2.1. Materials

Sodium borohydride ($NaBH_4$), zinc sulfide (ZnS) particles, iron (II) sulfate heptahydrate ($FeSO_4 \cdot 7H_2O$) and Lindane ($C_6H_6Cl_6$) were provided by Sigma–Aldrich. Syndiotactic polystyrene (sPS) used for the aerogels preparation was purchased from Idemitsu Kosan Co., Ltd. under the trademark XAREC© 90ZC.

2.2. Preparation of Fe^0 and Fe^0/ZnS *photocatalyst*

Fe^0/ZnS (FZ) photocatalyst in powder form were prepared following the procedure reported by Sacco et al. [39]. Specifically, 1 g of ZnS was added to 100 mL of distilled water where 4 g of $FeSO_4 \cdot 7H_2O$ was previously dissolved. The suspension was stirred for 10 minutes in the presence of an N_2 stream (flow rate: 30 NL/h) to remove dissolved oxygen. Subsequently, 1.4 g of reducing agent ($NaBH_4$) was added to the suspension, which was stirred in the presence of N_2 flow for 1 h, washed three

148 times with ethanol and finally dried at room temperature overnight to obtain the FZ
149 sample (Fe^0 content in the FZ photocatalyst was 45 wt % [39]).
150 Fe^0 particles were prepared following the same procedure but without adding ZnS in
151 the aqueous solution.
152 FZ, ZnS and Fe^0 particles were deeply characterized in our previous work [39]. In
153 detail, Wide-angle X-ray diffraction (WAXD) analysis of FZ evidenced diffraction
154 patterns (at 2θ= 28.6, 33.2, 47.6 and 56.5°) due to ZnS [67, 68]. Moreover, the
155 characteristic peak of Fe^0, at about $2\theta = 45°$, was also detectable [39] with no signals
156 related to iron oxides whose presence was instead shown by Raman spectra [39].
157
158 *2.3 Preparation of FZsPS monolithic composite aerogel*
159 The monolithic composite aerogel (FZsPS) was prepared according to the
160 experimental procedure described by Sacco et al. [66]. Syndiotactic polystyrene
161 (sPS) and the FZ photocatalyst with a weight ratio of 97/3 were dispersed in
162 chloroform (chloroform/sPS weight ratio equal to 90/10) and inserted in a
163 hermetically sealed test tube, which was then heated up to 100 °C. The formation of
164 a gel was obtained after cooling the suspension from 100°C to room temperature.
165 The chloroform was extracted from the obtained gel through treatment with
166 supercritical carbon dioxide (using an ISCO SFX 220 extractor) for 3 h at 40°C and
167 at a pressure of 20 MPa, obtaining the FZsPS monolithic composite aerogel in a
168 cylindrical shape (diameter=5.6 mm; height= 3 cm) (Figure S1 of Supplementary
169 Material).
170 The content of FZ photocatalyt inside the FZsPS composite was 3 wt%.

171 Only for toxicity data analysis, monolithic composite aerogels containing Fe^0 and
172 ZnS particles at 3 wt% (named Fe^0sPS and ZsPS, respectively) were also prepared
173 with the same method used for the preparation of FZsPS.

174 *2.4. Characterization techniques*

175 Wide-angle X-ray diffraction (WAXD) patterns of the photocatalysts were obtained
176 with a Brucker D8 Advance diffractometer, using a nickel filtered Cu-Kα radiation
177 and Bragg–Brentano θ–θ geometry. The 2θ acquisition interval was 5–80°, with a
178 step size of 0.0303° and a scanning acquisition time of 0.200 s/point.

179 To investigate the effect of iron on optical properties of ZnS powder, a Perkin Elmer
180 Spectrofluorometer LS55 was used to collect the photoluminescence spectra with an
181 excitation wavelength λex = 285 nm and slits 10 nm, recorded in the λ range of 300-
182 550 nm.

183 The specific surface area (SSA) of the composite aerogel was obtained by dynamic
184 N_2 adsorption measurements at −196 °C, using a Nova Quantachrome 4200e
185 instrument analyzer and evaluated by the BET method.

186 Field emission scanning electron microscopy (FE-SEM) enabled the morphological
187 analysis of the aerogel pellet. A ZEISS MERLIN instrument (Oberkochen, Germany)
188 was used; the samples were deposited on a carbon-coated stub and then coated with a
189 7 nm Pt layer.

190 In order to investigate the presence and distribution of FZ powders throughout the
191 aerogel sample, energy-dispersive X-ray spectroscopy (EDS) analyses by using
192 Aztec Software (Oxford Instruments) were performed on the same instrumentation.

193 Temperature programmed reduction (TPR-H_2) measurements were carried out in
194 AMI-300 (Altamira Instrument). The FZ sample was reduced in 5% H_2–95% Ar with

195 a flow rate of 50 Ncm^3 min^{-1} and a heating rate of 10°C min^{-1}. TPR-H_2 profile was
196 recorded using a thermo-conductive detector [69].
197
198 *2.5 Photocatalytic activity tests*
199 The photocatalytic tests were out carried in presence of UV light using a Pyrex
200 cylindrical reactor (ID = 3.5 cm, h = 28 cm, V = 269 mL). A UV-LEDs strip
201 (nominal power: 10 W, main wavelength emission: 365 nm, provided by LED
202 lighting hut, Shenzhen, China) was used as light source. The UV-LEDs strip was
203 placed around and in contact with the outer surface of the photoreactor. The
204 photocatalytic tests were performed on 100 mL of aqueous solution at a lindane
205 concentration of 100 μg/L and using a photocatalyst dosage equal to 0.09 g/L for FZ,
206 Fe^0 and ZnS in powder form, whereas the used FZsPS dosage was 3 g/L
207 (corresponding to an FZ dosage of 0.09 g/L). Fe^0 degradation efficiency was instead
208 analysed in the absence of light [39].
209 In the case of the tests with the FZsPS monolithic composite aerogel, a volume (2
210 mL) of solution was taken at different times to analyze the lindane concentration. In
211 the case of the tests with powder photocatalysts, before the analysis, the taken
212 suspension (2 mL) was filtered through 0.45 μm membrane to separate the
213 photocatalyst from the solution. An Agilent Gas Chromatograph (model 7820 A)
214 equipped with an Electron Capture Detector (ECD) was used to evaluate the lindane
215 concentration. The used analytical method was that one described by the EPA (U.S.
216 Environmental Protection Agency, SW-846 Test Method 8081B, Organochlorine
217 Pesticides by Gas Chromatography). The total organic carbon (TOC) of aqueous
218 solutions was measured with a TOC analyzer (Multi N/C 3100S, Analytik Jena),
219 which used an air flow of 160 Ncm^3/min and drew 500 μL per sample.

220 *2.6. Bioassays and toxicity data analysis*

221 The bioassays carried out with *Artemia franciscana* and data analysis were in
222 accordance with [70, 71]. Ten nauplii, metanauplii, and juvenile, and five adults
223 were exposed to increasing percentage concentrations of three experimental
224 conditions ((i) negative control – synthetic seawater (SSW, prepared in according to
225 ISO 10253/16) plus amendments (distilled water + FZ or distilled water + FZsPS);
226 (ii) positive control – seawater spiked with lindane (100 μg/L) (distilled water +
227 lindane) to check the toxic impact of lindane; (iii) seawater spiked with treatments
228 effluents (distilled water + lindane + Fe^0 or distilled water + lindane + FZ or distilled
229 water + lindane + FZsPS or distilled water + lindane + Fe^0sPS or distilled water +
230 lindane + ZsPS).
231 About RNA extraction and cDNA synthesis, two hundred nauplii and metanauplii,
232 one hundred juvenile and ten adults of *Artemia franciscana* were exposed to 100%
233 non-diluted aqueous solutions of distilled water + FZsPS, distilled water + lindane
234 and distilled water + lindane + FZsPS. All details about the experimental plan and
235 materials are provided in Supplementary Materials.

236

237 **3. Results and Discussion**

238 *3.1 Characterization results*

239 The WAXD results of the FZsPS aerogel (before and after use) and the FZ
240 photocatalyst in powder form are shown in Figure S2 of Supplementary Material.
241 The WAXD spectrum of bare sPS has been included for comparison.

242 The diffraction patterns of the FZsPS composite aerogel show both the diffraction
243 peaks of the δ crystalline form of sPS (2θ= 10 - 23.6°) [62] and of the crystalline

phase of ZnS (2θ= 28.6, 47.7, 56.6°) [39]. Moreover, the characteristic peak of Fe^0 (2θ = 45°) [39] is also detectable for both FZ and FZsPS composite aerogel, confirming the presence of FZ photocatalyst within the sPS matrix and evidencing that the inclusion of FZ particles within the polymer framework did not alter the δ crystalline form of sPS.

FZsPS specific surface area (SSA), evaluated by BET method, was 309 m^2/g, while for FZ photocatalyst in powder form and bare sPS, the SSA was 44 and 340 m^2/g, respectively. The observed slight reduction of the FZsPS composite SSA compared to that of bare sPS aerogel, as a result of the photocatalyst particle embedding within the sPS framework, is in agreement with SSA values commonly observed in sPS aerogel-based composite materials [39].

Morphological evaluation performed on the FZsPS aerogel by means of Field Emission Scanning Electron Microscopy (FESEM) confirmed the presence of FZ photocatalyst throughout the sample. FESEM images, shown in Figure 1, highlight the distribution and morphology of FZ powders in FZsPS aerogel.

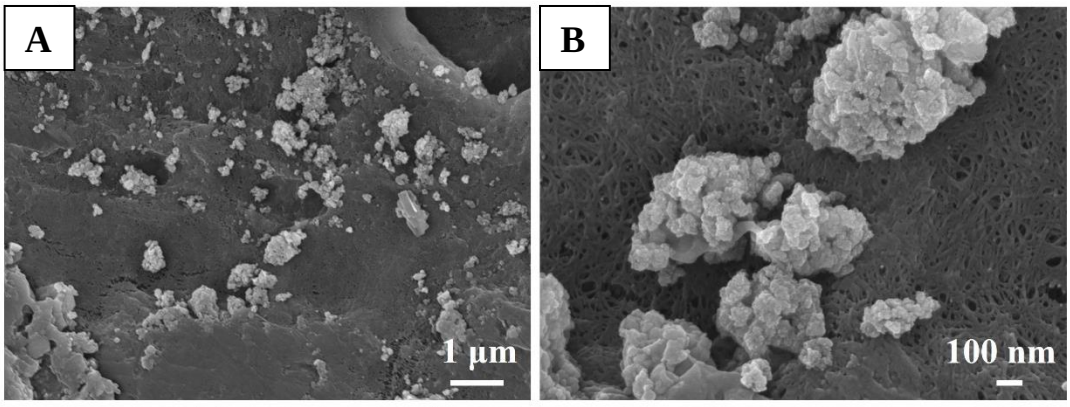

Figure 1: FESEM images of the FZsPS monolithic composite aerogel at two different magnifications.

At lower magnification (Figure 1A) the sample overview shows that FZ particles are well dispersed and incorporated into the polymer matrix, although particle agglomerates are also present in some areas. At higher magnification (Figure 1B) the morphology of FZ particles and porosity of the polymeric phase, having a fibrillar structure [66] are better highlighted. The FZ particle morphology observed in the composite, is different from that of the unsupported FZ powders (Figure S3 of Supplementary Material), characterized by sphere-like aggregates composed of flakes. This difference may be ascribed to the processing conditions involved during aerogel formation [72].

EDS analysis on the FZsPS composite aerogel sample was exploited to confirm the chemical composition of the material where the mapping of the different elements composing the catalyst powders enabled to explore their distribution onto the aerogel surface.

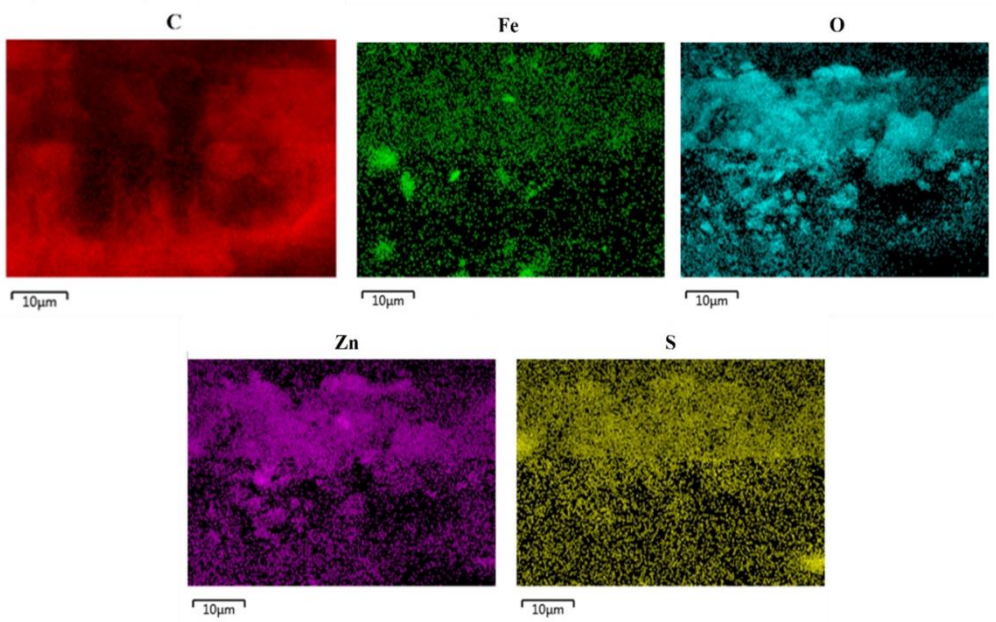

Figure 2: EDS analysis performed on the composite aerogel FZsPS. Mapping of Fe, O, C, Zn and S elements.

As shown in Figure 2, elements such as Zn, S, Fe and O were found in the FZ particle agglomerates, while C was localized in surrounding area corresponding to the sPS polymeric matrix. The mapping of Fe, Zn and S has highlighted both a homogeneous distribution of these elements and an interpenetration of them, although areas with higher Fe concentrations are also present. The homogeneous interpenetration of Fe and ZnS is in agreement with the distribution of elements observed in unsupported FZ powders (Figure S4 of Supplementary Material), where the EDS elemental analysis highlights the tendency of iron to organize itself in chain structures surrounding the ZnS, phase. Finally, the EDS mapping also evidenced greater concentrations of O in areas characterized by higher Fe concentrations, suggesting the possible presence of iron in its oxidized form.

In order to ascertain the presence of oxidised iron, the FZ sample was studied by means of the TPR technique. The TPR profile of FZ presents reduction peaks located at high temperature, 690 and 740°C (Figure 3). These peaks can be attributed exclusively to iron phases, in agreement with the results of Dutková et al [73]. Before 650°C no reduction peaks are detected, indicating that α-hematite like phase (Fe_2O_3) is not present. Considering the adopted heating ramp (10°C min^{-1}), the sharp peaks around 700°C are mainly attributed to the step reduction of the magnetite-like phase (Fe_3O_4) to metallic iron [74]. Correlating this result with the absence of peaks related to iron oxides from the WAXD analysis reported by Sacco et al. [39], we can speculate the presence of nonstoichiometric amorphous phases. The results obtained from TPR profile agree with the presence of iron oxides detected in the Raman spectrum of FZ reported in ref [39].

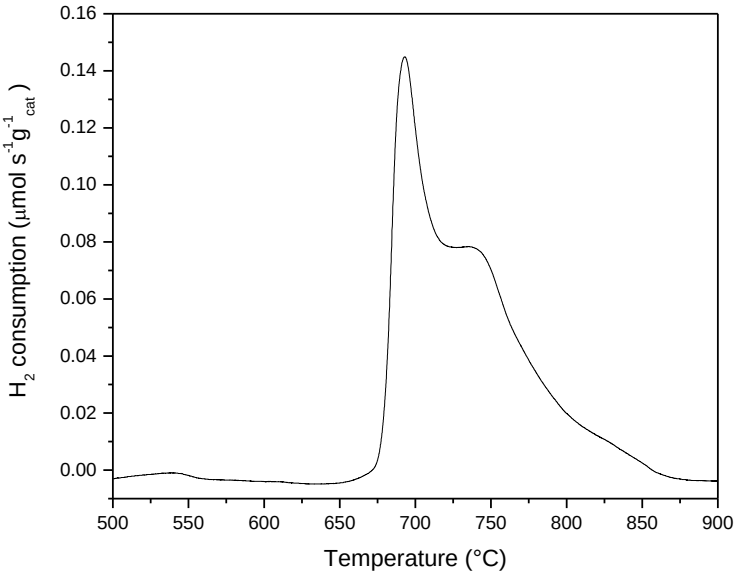

306

307 **Figure 3:** Temperature programmed reduction (TPR) profile of FZ photocatalyst.

308 Photoluminescence (PL) spectral analysis was conducted to verify the impact of iron
309 on the optical properties of the prepared photocatalyst.

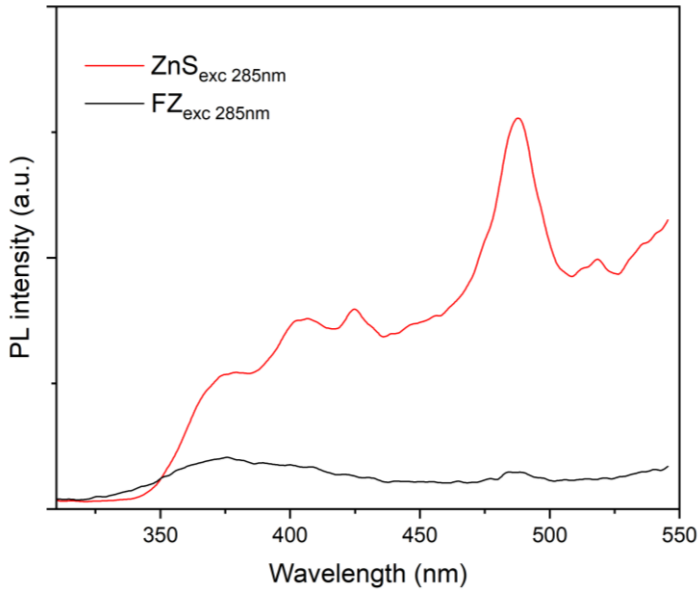

310
311 **Figure 4:** Photoluminescence spectra of modified and unmodified system: FZ and
312 ZnS.
313

314 Figure 4 shows the room temperature PL spectra, under 285 nm excitation, for pure
315 ZnS and FZ powder prepared as reported by Sacco et al. [39]. The PL spectrum of
316 ZnS shows a multipeak emission typical of this semiconductor [75]. The blue

emission band is attributed to defect states due to sulfur and zinc vacancies (about 425 and 480 nm, respectively). The broad emission band of peaks located between 360 nm and 405 nm is generally attributed to interstitial defects (S interstitial at low wavelength and Zn interstitial at higher wavelength) [76]. When the iron is introduced into the system, the PL peaks slightly shift to shorter wavelengths [77] but the main effect is the reduction of their intensity. The doping with iron allows to capture the photoactivated electrons and thus slows down the recombination between the valence and conduction bands, resulting in the decrease of PL intensity [78].

3.2 Photocatalytic activity results

The photocatalytic activity of commercial ZnS and FZ in powder form was evaluated in the degradation of lindane under UV light irradiation and compared with the degradation efficiency of Fe^0 in the absence of light (Figure 5). A sample-free control test, performed to verify the contribution of photolysis, showed no influence during the overall irradiation time, while a decrease in lindane relative concentration was found in the presence of ZnS, Fe^0 and FZ. In detail, with ZnS, the lindane concentration slowly decreased as a function of irradiation time, achieving a degradation efficiency of only about 35 % after 180 min. The low photocatalytic activity of ZnS could be explained considering that the C-Cl bonds of lindane structure are difficult to break by hydroxyl radicals generated when ZnS is excited by UV light [39, 79, 80], as also reported in some literature papers [33, 81, 82] in which it is shown that the photodegradation efficiency decreases by increasing the number of C-Cl bonds of the pollutants structure. Noticeably, in the absence of UV light, the lindane degradation efficiency by Fe^0 particles was higher than that of ZnS under irradiation, because of the high ability of Fe^0 to break the C-Cl bond of chlorinated organic pollutants [39, 83], leading to the complete lindane degradation in 180 min.

It is worth to pointing out that, under UV light, the lindane degradation by FZ photocatalyst was enhanced, showing faster degradation kinetics as compared with Fe^0 alone. Indeed, in the presence of FZ photocatalyst and UV light, the lindane relative concentration was always lower than that achieved with the non-irradiated Fe^0 particles. It is argued that the higher lindane degradation efficiency of FZ photocatalyst under UV light is due to the continuous reduction of Fe^{2+} (continuously generated from the reductive cleavage of C-Cl bonds by Fe^0) to Fe^0 by the electrons promoted in the conduction band of photoexcited ZnS, similarly to what reported for the photocatalytic degradation of chlorobenzene in presence of Fe^0/ZnS [39]. This assumption is consistent with the outcomes of photoluminescence analyses, which show a decrease in the electron-hole recombination rate for sample FZ.

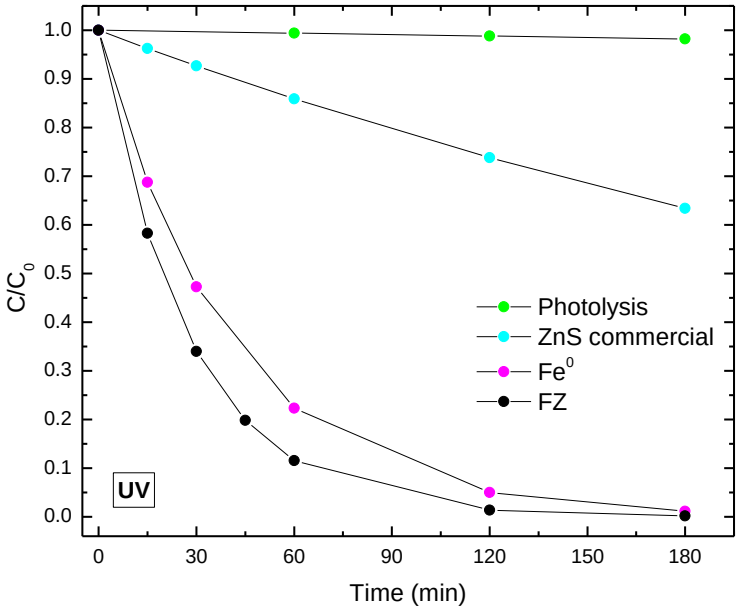

Figure 5: Photocatalytic degradation of lindane by ZnS and FZ under UV light irradiation and in the presence of Fe^0 in the absence of light.

Figure 6 reports the comparison of the lindane photocatalytic degradation obtained in the presence of FZ photocatalyst in powder form and FZsPS monolithic composite

360 aerogel.

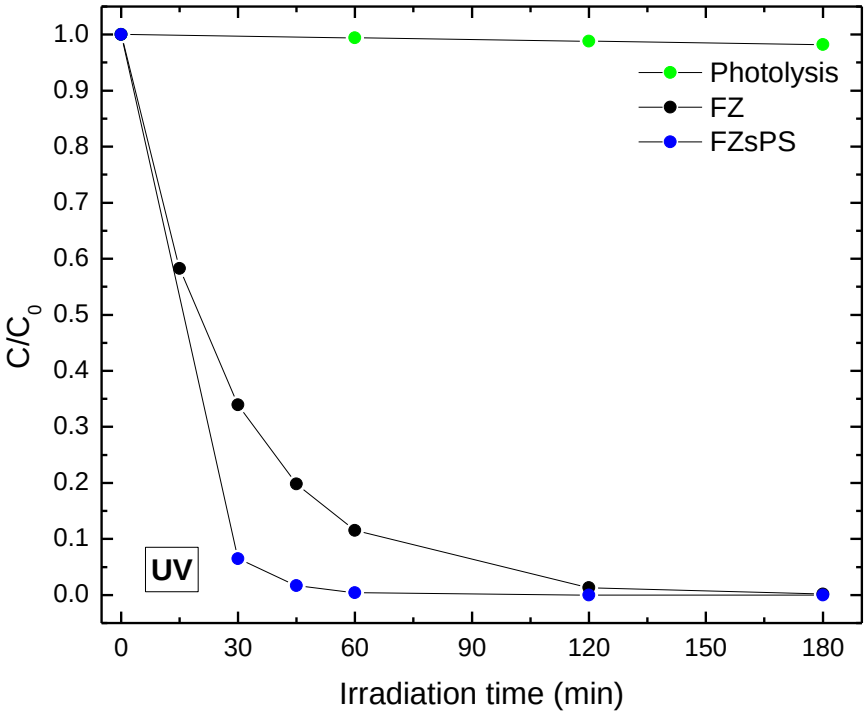

361

362 **Figure 6:** Photocatalytic degradation of lindane by FZ and FZsPS under UV light
363 irradiation.
364

365 Despite both FZ powder and FZsPS composite completely degraded lindane after
366 180 min of UV irradiation, the decreasing rate of lindane relative concentration as a
367 function of irradiation time clearly evidenced a photodegradation activity of FZsPS
368 significantly higher than that observed in the presence of FZ photocatalyst. Indeed,
369 using the FZsPS aerogel, the lindane degradation was about 95% after only 30 min
370 of irradiation time whereas the FZ photocatalyst exhibited a lindane degradation of
371 about 65% after the same irradiation time. These data underline that the
372 photodegradation activity is strongly promoted when the FZ photocatalyst in powder
373 form is dispersed in the polymer matrix.

374 The enhanced photocatalytic activity observed in the presence of FZsPS could be due
375 to the higher SSA of FZsPS (309 m^2/g) with respect to FZ (44 m^2/g) but also to the

affinity of lindane with the non-polar polymer matrix, which results in a concentration of lindane in the matrix itself. To confirm such hypothesis, an additional experiment was carried out to measure the amount of lindane absorbed by bare sPS monolithic aerogel in dark conditions performed with the same experimental conditions used for the photodegradation tests (solution volume: 100 mL; initial lindane concentration: 100 μg/L; sPS dosage: 3 g/L). (Figure S5 of Supplementary Materials). sPS aerogel showed an uptake of 30 % after 180 min. This result confirms the good affinity of the polymer matrix towards non-polar organic compounds (such as lindane), in agreement with the available literature [61, 65, 84, 85]. Therefore, it is possible to argue that the higher photodegradation efficiency of FZsPS aerogel is mainly due to the lindane absorption ability of the polymer matrix since the number of lindane molecules in contact with FZ particles embedded into sPS aerogel is increased. Thus, the photocatalytic degradation rate is enhanced.

The aqueous solution recovered after the photocatalytic treatment with the FZsPS aerogel was analysed by inductively coupled plasma optical emission spectrometry (ICP-OES Optima 7000DV, PerkinElmer). This analysis revealed the almost total absence of Fe (<0.01 mg/l) and a slight presence of Zn (3 mg/L), probably due to the partial leaching of the FZ particles immobilized on the external surface of sPS and not of those dispersed within the polymer framework.

To test whether such leaching phenomenon could negatively affect the stability of the FZsPS aerogel, photocatalytic experiments were repeated six times (Figure 7) using the same FZsPS monolithic composite aerogel and without any regeneration step of the photocatalyst.

The obtained results did not evidence any significant decrease in the lindane

photocatalytic degradation performance, demonstrating the stability and the possibility of reusing the FZsPS aerogel. Furthermore, WAXD analysis was performed on the FZsPS composite aerogel recovered from the photoreactor after the sixth reuse cycle. The obtained result is shown in Figure S2 of Supplementary Material. No substantial difference with respect to the WAXD spectrum of FZsPS before its use in the photocatalytic degradation of lindane was observed.

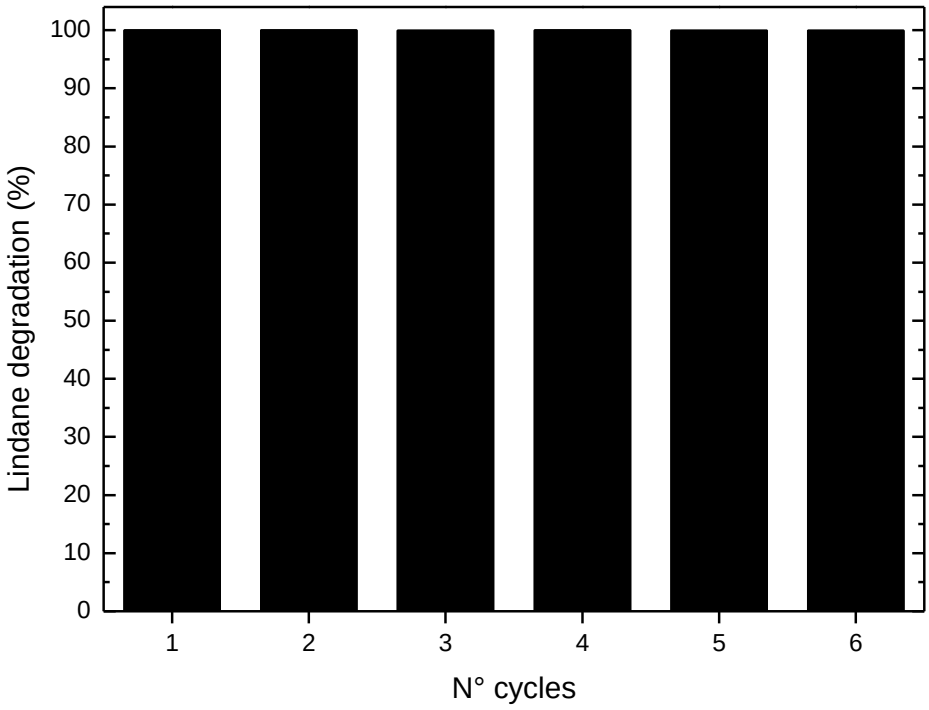

Figure 7: Lindane degradation after 180 min of UV irradiation using FZsPS aerogel in six reuse cycles.

An additional photocatalytic test was carried out with the FZsPS monolithic composite at a higher concentration of the pollutant (10 mg/L). The results were comparable to the test at a concentration of 100 μg/L (Figure 8).

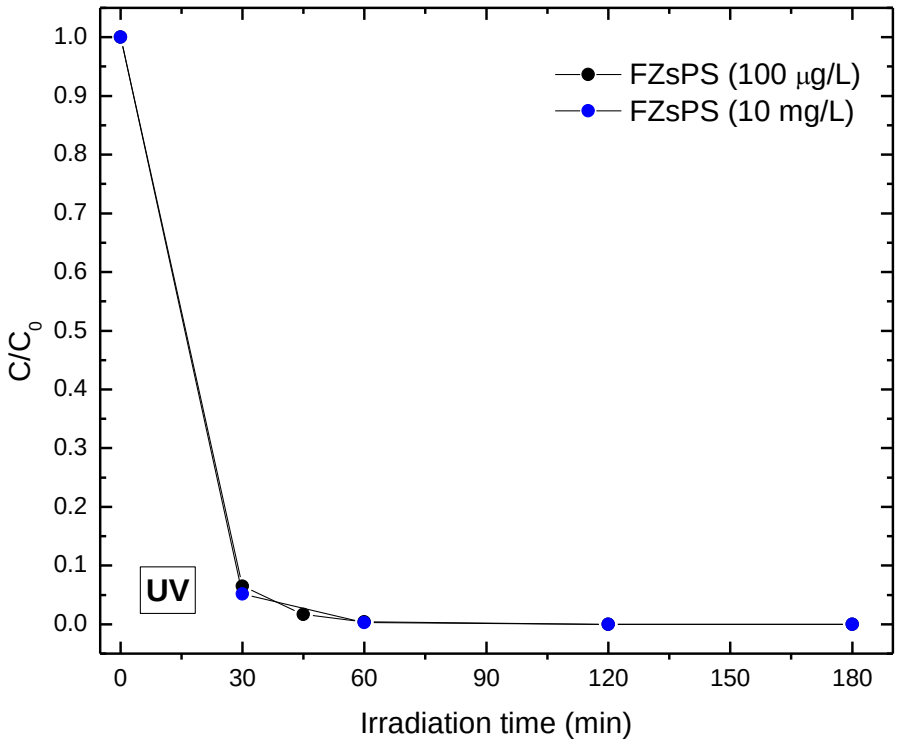

414

415 **Figure 8:** Photocatalytic degradation at two different lindane initial concentrations
416 (100 μg/L and 10 mg/L) by FZsPS under UV light irradiation.
417

418 For both initial lindane concentrations, a TOC removal of about 94% after 180
419 minutes of UV irradiation was achieved, underlining the strong ability of FZsPS in
420 the mineralization of lindane. Considering the literature findings concerning the
421 photoactivity of Fe^0/ZnS in powder form [39], it is possible to argue that the holes
422 generated in the ZnS valence band promote the formation of hydroxyl radicals,
423 which further oxidize the organic intermediates (such as benzene and cyclohexene
424 [86, 87]) generated from the cleavage of C-Cl bonds of lindane structure by Fe^0
425 supported on ZnS surface, leading to the almost complete TOC removal from
426 aqueous solution.

427 The photocatalytic degradation efficiency of the FZsPS monolithic composite
428 aerogel was compared with the performance of photocatalysts immobilized on
429 different supports and tested in the lindane photodegradation (Table 1).

Table 1: Comparison with literature papers dealing with different immobilized photocatalysts for lindane degradation.

Photoactive phase	Support	Light source	Lindane degradation (%)	Treatment time	Ref
TiO_2	Hollow glass microspheres	UV	68	30 min	[27]
N-doped TiO_2	Pyrex glass tube	UVA	~ 20	30 min	[30]
ZnO	Bio-nano hybrid system (*Candida* VITJzN04).	Sunlight	~ 70	24 h*	[31]
CeO_2–TiO_2	Stainless steel substrates	Simulated solar light	~ 50	2 h*	[88]
Fe^0/ZnS	sPS aerogel	UVA	~ 95	30	This paper

*no data at 30 min is available

It is worth noting to underline that the literature about lindane degradation by immobilized photocatalysts is very scarce. However, from the data reported in Table 1, it is possible to observe that the FZsPS monolithic composite aerogel used in our study shows the best performance in lindane degradation since an efficiency of 95 % is reached after only 30 min of irradiation time.

3.3. Toxicity results

As reported in Figure 9, after 48 h of exposure to different percentages of aqueous solutions of FZsPS, an increase of nauplii, metanauplii, juvenile and adult mortality (about 20%) was observed only at higher tested percentages, represented by 50% and 100%. These data were statistically significant with respect to the control and the others used concentrations ($p < 0.0001$; see Table S1 of Supplementary Material).

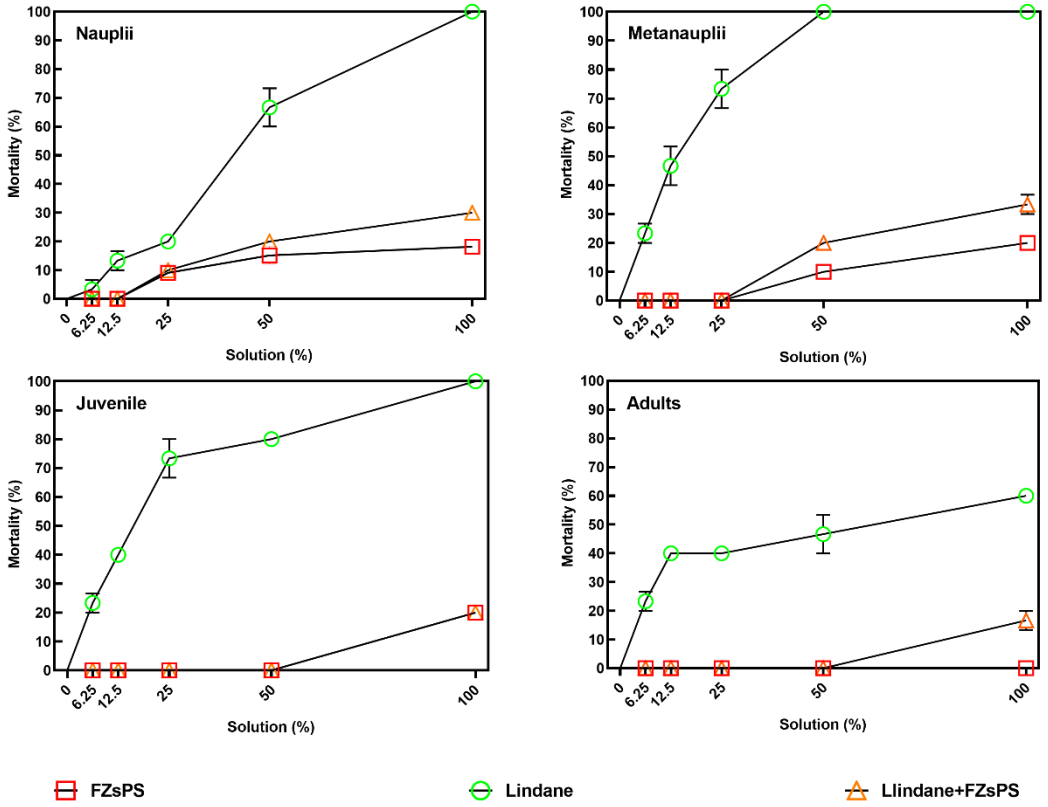

Figure 9: After 48 h, the percentage of dead nauplii, metanauplii, juvenile and adults detected both in control (0%) and treated samples with 6.25%, 12.5%, 25%, 50%, and 100% of FZsPS solution (distilled water+ FZsPS), Lindane solution (100 µg/L), Lindane + FZsPS (Treated effluents after 180 min of UV irradiation). Data are reported as a mean ± standard deviation.

Lindane solution (100 µg/L) caused mortality (about 10-20%) in all life stages already at 6.25% that was statistically significant with respect to the control and all other concentrations ($p < 0.0001$; Figure 9; Table S1). Except for adults, the mortality in all life stages at 100% solution involved all organisms.

Considering nauplii and metanauplii exposure to treated effluent (Lindane + FZsPS) (Figure 9), a low percentage of about 20% of dead was observed at 50%. At 100%, a significant increase of toxicity (about 30%) compared to lower (0%, 6.25%, 12.5%, and 25%; $p < 0.0001$) and higher concentrations (50%; $p < 0.01$) was detected.

462 Considering juvenile and adult exposure to the same condition, a low percentage of
463 about 20% of death was observed only at 100%. These data were statistically
464 significant compared to the control and all other concentrations ($p < 0.0001$; see also
465 Table S1).
466 Only the 50% and 100% of FZ and treated effluent by FZ (Lindane +FZ)
467 (Supplementary Figure S6), caused a significant increase of toxicity in four different
468 life stage (about 20% and 30%, respectively) with respect all tested concentrations (p
469 < 0.0001).
470 Taking into the consideration nauplii and metanauplii exposure to treated effluent by
471 Fe^0 (Lindane + Fe^0) at 25% (Figure S6), a significant percentage of mortality (about
472 20% and 35%, respectively) was observed respecting lower (0%, 6.25%, 12.5%; $p<$
473 0.0001). At 50% and 100%, a significant increase in toxicity (about 40-50%) was
474 shown respecting all tested concentrations ($p< 0.0001$). Considering juvenile and
475 adult exposure, only at 100%, Lindane + Fe^0 solution caused a significant increase in
476 mortality (about 40%) with respect to all tested concentrations ($p < 0.0001$).
477 Finally, Lindane + Fe^0sPS and Lindane + ZsPS treated effluents (Figure S6) were
478 able to significantly impact the survival of *Artemia* only at 100% with respect to all
479 tested concentrations ($p < 0.0001$; see also Table S1).
480
481 *3.4. Effects of FZsPS on gene expression by real-time qPCR*
482 The expression levels of five genes (Albarano et al., 2022a), involved in stress
483 response, were followed by real-time qPCR after FZsPS treatment experiment
484 (Figure 10; see also Table S2 for the values).

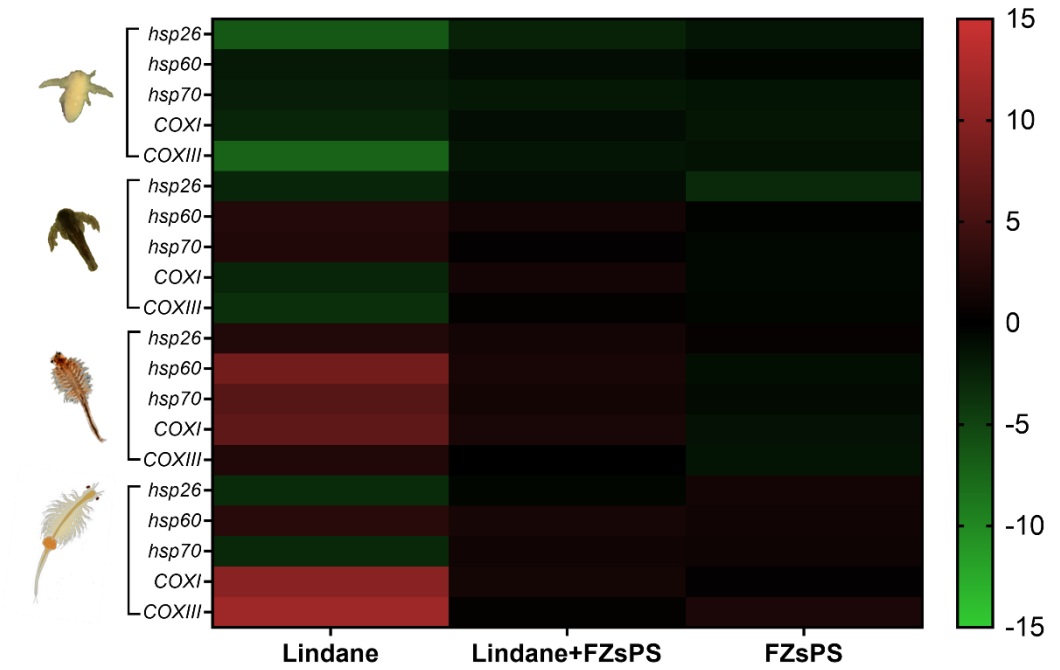

Figure 10: Heatmap showing the expression profiles and hierarchical clustering of five genes analyzed through real-time qPCR in nauplii, metanauplii, juvenile and adult treated with FZsPS solution (distilled water+ FZsPS), Lindane (100 µg/L), Lindane + FZsPS (Treated effluents after 180 min of UV irradiation). Color code: red, up-regulated genes with respect to the control; green, down-regulated genes with respect to the control; black, genes for which there was no variation in expression with respect to the control.

All analyzed genes were targeted in all life stages after lindane exposure with the exception of *hsp60*. Specifically, *hsp26* was down-regulated in nauplii, metanauplii and adult (6.40-fold 2.78-fold and 3.20-fold, respectively) and up-regulated in juvenile (2.46-fold; see Table S2); *hsp70* was down-regulated in nauplii and adult (2.19-fold and 2.87-fold, respectively) and up-regulated in metanauplii and juvenile (2.28-fold and 6.32-fold, respectively); *COXI* and *COXIII* were down-regulated in nauplii (2.77-fold and 7.28-fold, respectively) and metanauplii (2.73-fold and 3.50-fold, respectively) and up-regulated in juvenile (6.91-fold and 2.30-fold,

501 respectively) and adult (9.96-fold and 11.54-fold, respectively; Table S2); *hsp60* was
502 up-regulated in metanauplii, juvenile and adult (2.50-fold, 8.30-fold and 2.90-fold,
503 respectively; see Table S2).
504 Considering other treatments (Figure 10), *hsp60* was down-regulated (2.55-fold)
505 only in nauplii after the exposure to the treated effluent (lindane + FZsPS), and
506 *hsp26* was down-regulated (3.01-fold) only in metanauplii after the exposure to
507 FZsPS solution (distilled water + FZsPS) (Table S2).
508

509 **4. Conclusions**

510 In this work, a monolithic composite aerogel based on sPS and Fe^0/ZnS (FZsPS) was
511 tested, for the first time, as a photocatalyst to achieve the complete lindane
512 degradation under UV light. Fe/ZnS powder is well dispersed throughout the
513 polymer matrix even if agglomerates are present and emerge from the surface, as
514 evident from FESEM images and EDS analysis. The mapping of the different
515 elements (Fe, Zn, S, O, C) showed diffuse Fe chain structures interpenetrated with
516 ZnS particles, although iron oxides, in accordance with TPR analyses, were also
517 detected.

518 The photodegradation performance of FZsPS was significantly higher than that
519 observed in the presence of Fe^0/ZnS photocatalyst in powder form (FZ). In detail,
520 using the FZsPS monolithic composite aerogel, the almost complete lindane
521 degradation was achieved after only 30 min of irradiation time whereas the FZ
522 photocatalyst exhibited a lindane degradation of about 65% after the same irradiation
523 time. Moreover, a TOC removal of about 94% after 180 minutes of UV irradiation
524 was achieved, underlining the ability of FZsPS also in the lindane mineralization.
525 The enhanced photocatalytic activity observed in the presence of FZsPS aerogel is

due to the higher SSA of FZsPS (309 m^2/g) with respect to FZ (44 m^2/g) but also to the concentration of lindane in the sPS matrix. Reusability studies performed on FZsPS showed no significant decrease in the photocatalytic activity, demonstrating the stability of the formulated monolithic composite aerogel. Moreover, the effluent from the photocatalytic treatment based on FZsPs composite aerogel can be considered at low risk of environmental impact since no significant toxic effects on *Artemia franciscana* were evidenced. Therefore, based on the ecotoxicity results, the strategy of dispersing the ZVI/ZnS catalyst in a highly porous polymeric matrix, such as sPS aerogel, can be considered as a model for using otherwise harmful catalysts in water remediation.

Acknowledgements

Authors thank Dr Marco Allione (Politecnico di Torino, Italy) for FESEM measurements on Fe^0/ZnS photocatalyst, Dr. Mariagrazia Napoli and Dr. Ivano Immediata (University of Salerno, Italy) for the technical assistance in gas chromatographic analysis. Authors also thank Dr. Patrizia Iannece (University of Salerno, Italy) for the ICP-OES analysis of water recovered after the photocatalytic treatment.

References

[1] L.R.E.D. RED, Docket Control Number OPP-2002-0202 Lindane Reregistration Eligibility Decision (RED) Comments Submitted on Behalf of the Natural Resources Defense Council By Gina M. Solomon, MD, MPH Senior Scientist, NRDC, (2002).
[2] H. Fu, X. Quan, Z. Liu, S. Chen, Photoinduced transformation of γ-HCH in the presence of dissolved organic matter and enhanced photoreactive activity of humate-coated α-Fe2O3, Langmuir, 20 (2004) 4867-4873.
[3] G. Marko, M. Snezana, B. Jelena, K. Marijana, R. Srdjan, T. Aleksandra, A. Jasmina, Lindane and hexachlorobenzene sequestration and detoxification in contaminated sediment amended with carbon-rich sorbents, Chemosphere, (2019).

[4] W.H. Organization, Lindane (gamma-HCH: health and safety guide, (1991).
[5] J. Vijgen, The Legacy of Lindane HCH Isomer Production: A Global Overview of Residue Management, Formulation and Disposal: Main Report. Annexes, International HCH & Pesticides Association, 2006.
[6] M. Vega, D. Romano, E. Uotila, Lindane (Persistant Organic Pollutant) in the EU, Best Practices of De-Contamination Exchanged, (2016).
[7] W.H. Organization, Pesticide Residues in Food-2003: Evaluations, Food & Agriculture Org., 2004.
[8] J.C. Hansen, L.-O. Reiersen, S. Wilson, Arctic Monitoring and Assessment Programme (AMAP); strategy and results with focus on the human health assessment under the second phase of AMAP, 1998–2003, in, Taylor & Francis, 2002.
[9] M. Gmurek, M. Olak-Kucharczyk, S. Ledakowicz, Photochemical decomposition of endocrine disrupting compounds–A review, Chemical Engineering Journal, 310 (2017) 437-456.
[10] J.O. Babayemi, Overview of levels of organochlorine pesticides in surface water and food items in Nigeria, Journal of Environment and Earth Science, 6 (2016) 77-86.
[11] V. Nagpal, A.D. Bokare, R.C. Chikate, C.V. Rode, K.M. Paknikar, Reductive dechlorination of γ-hexachlorocyclohexane using Fe–Pd bimetallic nanoparticles, Journal of hazardous materials, 175 (2010) 680-687.
[12] J. Vijgen, P. Abhilash, Y.F. Li, R. Lal, M. Forter, J. Torres, N. Singh, M. Yunus, C. Tian, A. Schäffer, Hexachlorocyclohexane (HCH) as new Stockholm Convention POPs—a global perspective on the management of Lindane and its waste isomers, Environmental Science and Pollution Research, 18 (2011) 152-162.
[13] B.R. Shah, U.D. Patel, Mechanistic aspects of photocatalytic degradation of Lindane by TiO2 in the presence of Oxalic acid and EDTA as hole-scavengers, Journal of Environmental Chemical Engineering, 9 (2021) 105458.
[14] S. Wacławek, D. Silvestri, P. Hrabák, V.V. Padil, R. Torres-Mendieta, M. Wacławek, M. Černík, D.D. Dionysiou, Chemical oxidation and reduction of hexachlorocyclohexanes: A review, Water research, 162 (2019) 302-319.
[15] S. Deng, N. Feng, S. Kang, J. Zhu, B. Yu, J. Chen, X. Xie, Mechanochemical formation of chlorinated phenoxy radicals and their roles in the remediation of hexachlorobenzene contaminated soil, Journal of Hazardous Materials, 352 (2018) 172-181.
[16] I. San Román, A. Galdames, M. Alonso, L. Bartolomé, J. Vilas, R. Alonso, Effect of coating on the environmental applications of zero valent iron nanoparticles: the lindane case, Science of the Total Environment, 565 (2016) 795-803.
[17] X. Zhu, Y. Li, B. Han, Q. Feng, L. Zhou, Degradation Characteristics of Carbon Tetrachloride by Granular Sponge Zero Valent Iron, International Journal of Environmental Research and Public Health, 18 (2021) 12578.
[18] S. Bajaj, S. Sagar, S. Khare, D.K. Singh, Biodegradation of γ-hexachlorocyclohexane (lindane) by halophilic bacterium Chromohalobacter sp. LD2 isolated from HCH dumpsite, International Biodeterioration & Biodegradation, 122 (2017) 23-28.
[19] F.O. Kengara, U. Doerfler, G. Welzl, B. Ruth, J.C. Munch, R. Schroll, Enhanced degradation of 14C-HCB in two tropical clay soils using multiple anaerobic–aerobic cycles, Environmental pollution, 173 (2013) 168-175.

603 [20] J.F. Devlin, J. Klausen, R.P. Schwarzenbach, Kinetics of nitroaromatic
604 reduction on granular iron in recirculating batch experiments, Environmental science
605 & technology, 32 (1998) 1941-1947.
606 [21] H.-J. Lu, J.-K. Wang, S. Ferguson, T. Wang, Y. Bao, H.-x. Hao, Mechanism,
607 synthesis and modification of nano zerovalent iron in water treatment, Nanoscale, 8
608 (2016) 9962-9975.
609 [22] T. Pasinszki, M. Krebsz, Synthesis and application of zero-valent iron
610 nanoparticles in water treatment, environmental remediation, catalysis, and their
611 biological effects, Nanomaterials, 10 (2020) 917.
612 [23] W. Shen, X. Wang, F. Jia, Z. Tong, H. Sun, X. Wang, F. Song, Z. Ai, L. Zhang,
613 B. Chai, Amorphization enables highly efficient anaerobic thiamphenicol reduction
614 by zero-valent iron, Applied Catalysis B: Environmental, 264 (2020) 118550.
615 [24] W. Xu, Z. Li, S. Shi, J. Qi, S. Cai, Y. Yu, D.M. O'Carroll, F. He,
616 Carboxymethyl cellulose stabilized and sulfidated nanoscale zero-valent iron:
617 Characterization and trichloroethene dechlorination, Applied Catalysis B:
618 Environmental, 262 (2020) 118303.
619 [25] V. Vaiano, O. Sacco, M. Matarangolo, Photocatalytic degradation of
620 paracetamol under UV irradiation using TiO2-graphite composites, Catalysis Today,
621 315 (2018) 230-236.
622 [26] S. Khan, C. Han, M. Sayed, M. Sohail, S. Jan, S. Sultana, H.M. Khan, D.D.
623 Dionysiou, Exhaustive photocatalytic lindane degradation by combined simulated
624 solar light-activated nanocrystalline TiO2 and inorganic oxidants, Catalysts, 9 (2019)
625 425.
626 [27] A. Zaleska, J. Hupka, M. Wiergowski, M. Biziuk, Photocatalytic degradation of
627 lindane, p, p′-DDT and methoxychlor in an aqueous environment, Journal of
628 photochemistry and photobiology A: chemistry, 135 (2000) 213-220.
629 [28] H.J. Jung, R. Koutavarapu, S. Lee, J.H. Kim, H.C. Choi, M.Y. Choi, Enhanced
630 photocatalytic degradation of lindane using metal–semiconductor Zn@ ZnO and
631 ZnO/Ag nanostructures, Journal of Environmental Sciences, 74 (2018) 107-115.
632 [29] D.-K. Lee, I.-C. Cho, Characterization of TiO2 thin film immobilized on glass
633 tube and its application to PCE photocatalytic destruction, Microchemical journal, 68
634 (2001) 215-223.
635 [30] J. Senthilnathan, L. Philip, Photocatalytic degradation of lindane under UV and
636 visible light using N-doped TiO2, Chemical engineering journal, 161 (2010) 83-92.
637 [31] J.A. Salam, N. Das, Degradation of lindane by a novel embedded bio-nano
638 hybrid system in aqueous environment, Applied microbiology and biotechnology, 99
639 (2015) 2351-2360.
640 [32] T.S. Jamil, E.S. Mansor, R.A. Nasr, Degradation of Lindane using two
641 nanosized BiOXs and their heterojunction under visible light, Desalination and
642 Water Treatment, 57 (2016) 14750-14761.
643 [33] S. Khan, C. Han, H.M. Khan, D.L. Boccelli, M.N. Nadagouda, D.D. Dionysiou,
644 Efficient degradation of lindane by visible and simulated solar light-assisted S-
645 TiO2/peroxymonosulfate process: kinetics and mechanistic investigations, Molecular
646 Catalysis, 428 (2017) 9-16.
647 [34] X. Wang, M. Hong, F. Zhang, Z. Zhuang, Y. Yu, Recyclable nanoscale zero
648 valent iron doped g-C3N4/MoS2 for efficient photocatalysis of RhB and Cr (VI)
649 driven by visible light, ACS Sustainable Chemistry & Engineering, 4 (2016) 4055-
650 4063.

[35] X. Wang, D. Lizong, Well-dispersed zero-valent iron supported on Fe 3 O 4/gC 3 N 4 composites via a facile approach with versatile photoredox catalysis, Journal of Nanoparticle Research, 20 (2018) 1-15.
[36] C. Huang, W.-P. Hsieh, J.R. Pan, S.-M. Chang, Characteristic of an innovative TiO2/Fe0 composite for treatment of azo dye, Separation and Purification Technology, 58 (2007) 152-158.
[37] K. Kobwittaya, S. Sirivithayapakorn, Photocatalytic reduction of nitrate over Fe-modified TiO2, APCBEE procedia, 10 (2014) 321-325.
[38] Y. Liu, J. Wang, Reduction of nitrate by zero valent iron (ZVI)-based materials: A review, Science of the Total Environment, 671 (2019) 388-403.
[39] O. Sacco, V. Vaiano, W. Navarra, C. Daniel, S. Pragliola, V. Venditto, Catalytic system based on recyclable Fe0 and ZnS semiconductor for UV-promoted degradation of chlorinated organic compounds, Separation and Purification Technology, 270 (2021) 118830.
[40] D. Friedmann, A General Overview of Heterogeneous Photocatalysis as a Remediation Technology for Wastewaters Containing Pharmaceutical Compounds, Water, 14 (2022) 3588.
[41] S.K. Loeb, P.J. Alvarez, J.A. Brame, E.L. Cates, W. Choi, J. Crittenden, D.D. Dionysiou, Q. Li, G. Li-Puma, X. Quan, The technology horizon for photocatalytic water treatment: sunrise or sunset?, in, ACS Publications, 2018.
[42] R. Ata, O. Sacco, V. Vaiano, L. Rizzo, G.Y. Tore, D. Sannino, Visible light active N-doped TiO2 immobilized on polystyrene as efficient system for wastewater treatment, Journal of Photochemistry and Photobiology A: Chemistry, 348 (2017) 255-262.
[43] V. Vaiano, G. Sarno, O. Sacco, D. Sannino, Degradation of terephthalic acid in a photocatalytic system able to work also at high pressure, Chemical Engineering Journal, 312 (2017) 10-19.
[44] I. Zammit, R.B. Marano, V. Vaiano, E. Cytryn, L. Rizzo, Changes in antibiotic resistance gene levels in soil after irrigation with treated wastewater: a comparison between heterogeneous photocatalysis and chlorination, Environmental Science & Technology, 54 (2020) 7677-7686.
[45] O. Sacco, M. Matarangolo, V. Vaiano, G. Libralato, M. Guida, G. Lofrano, M. Carotenuto, Crystal violet and toxicity removal by adsorption and simultaneous photocatalysis in a continuous flow micro-reactor, Science of the total environment, 644 (2018) 430-438.
[46] D. Minetto, G. Libralato, A.V. Ghirardini, Ecotoxicity of engineered TiO2 nanoparticles to saltwater organisms: an overview, Environment international, 66 (2014) 18-27.
[47] B.M. Rotoli, P. Guidi, B. Bonelli, M. Bernardeschi, M.G. Bianchi, S. Esposito, G. Frenzilli, P. Lucchesi, M. Nigro, V. Scarcelli, Imogolite: an aluminosilicate nanotube endowed with low cytotoxicity and genotoxicity, Chemical Research in Toxicology, 27 (2014) 1142-1154.
[48] V. Addorisio, D. Pirozzi, S. Esposito, F. Sannino, Decontamination of waters polluted with simazine by sorption on mesoporous metal oxides, Journal of hazardous materials, 196 (2011) 242-247.
[49] F. Tescione, O. Tammaro, A. Bifulco, G. Del Monaco, S. Esposito, M. Pansini, B. Silvestri, A. Costantini, Silica meets tannic acid: Designing green nanoplatforms for environment preservation, Molecules, 27 (2022) 1944.

[50] T. McMurray, P. Dunlop, J. Byrne, The photocatalytic degradation of atrazine on nanoparticulate TiO2 films, Journal of Photochemistry and Photobiology A: Chemistry, 182 (2006) 43-51.
[51] M. Karavasilis, M. Theodoropoulou, C. Tsakiroglou, Degradation of the persistent organic pollutant-lindane in fixed-bed photoreactor packed with immobilized Zinc Oxide and Iron oxide-doped Zinc Oxide photocatalysts, in: IOP Conference Series: Earth and Environmental Science, IOP Publishing, 2022, pp. 012082.
[52] V. Venditto, M. Pellegrino, R. Califano, G. Guerra, C. Daniel, L. Ambrosio, A. Borriello, Monolithic polymeric aerogels with VOCs sorbent nanoporous crystalline and water sorbent amorphous phases, ACS applied materials & interfaces, 7 (2015) 1318-1326.
[53] C. Daniel, M. Pellegrino, V. Venditto, S. Aurucci, G. Guerra, Nanoporous-crystalline poly (2, 6-dimethyl-1, 4-phenylene) oxide (PPO) aerogels, Polymer, 105 (2016) 96-103.
[54] G. Balasubramanian, D.D. Dionysiou, M.T. Suidan, I. Baudin, J.-M. Laıné, Evaluating the activities of immobilized TiO2 powder films for the photocatalytic degradation of organic contaminants in water, Applied Catalysis B: Environmental, 47 (2004) 73-84.
[55] S. Suárez, J.M. Coronado, R. Portela, J.C. Martín, M. Yates, P. Avila, B. Sánchez, On the preparation of TiO2− sepiolite hybrid materials for the photocatalytic degradation of TCE: influence of TiO2 distribution in the mineralization, Environmental science & technology, 42 (2008) 5892-5896.
[56] O. Sacco, V. Vaiano, M. Matarangolo, ZnO supported on zeolite pellets as efficient catalytic system for the removal of caffeine by adsorption and photocatalysis, Separation and Purification Technology, 193 (2018) 303-310.
[57] S. Singh, H. Mahalingam, P.K. Singh, Polymer-supported titanium dioxide photocatalysts for environmental remediation: A review, Applied Catalysis A: General, 462 (2013) 178-195.
[58] M.J. Silva, J. Gomes, P. Ferreira, R.C. Martins, An overview of polymer-supported catalysts for wastewater treatment through light-driven processes, Water, 14 (2022) 825.
[59] W. Navarra, O. Sacco, C. Daniel, V. Venditto, V. Vaiano, D.A.L. Vignati, C. Bojic, G. Libralato, G. Lofrano, M. Carotenuto, Photocatalytic degradation of atrazine by an N-doped TiO2/polymer composite: catalytic efficiency and toxicity evaluation, Journal of Environmental Chemical Engineering, 10 (2022) 108167.
[60] S. Pragliola, R. De Vita, P. Longo, Aqueous emulsion polymerization of styrene and substituted styrenes using titanocene compounds, Polymer, 54 (2013) 1583-1587.
[61] C. Daniel, S. Longo, R. Ricciardi, E. Reverchon, G. Guerra, Monolithic nanoporous crystalline aerogels, Macromolecular rapid communications, 34 (2013) 1194-1207.
[62] V. Vaiano, O. Sacco, D. Sannino, P. Ciambelli, S. Longo, V. Venditto, G. Guerra, N-doped TiO2/s-PS aerogels for photocatalytic degradation of organic dyes in wastewater under visible light irradiation, Journal of Chemical Technology & Biotechnology, 89 (2014) 1175-1181.
[63] A. Mancuso, V. Vaiano, P. Antico, O. Sacco, V. Venditto, Photoreactive polymer composite for selective oxidation of benzene to phenol, Catalysis Today, 413 (2023) 113914.

[64] W. Navarra, O. Sacco, V. Venditto, V. Vaiano, Selective Photocatalytic Reduction of Nitrobenzene to Aniline Using TiO2 Embedded in sPS Aerogel, Polymers, 15 (2023) 359.
[65] O. Sacco, V. Vaiano, C. Daniel, W. Navarra, V. Venditto, Highly robust and selective system for water pollutants removal: How to transform a traditional photocatalyst into a highly robust and selective system for water pollutants removal, Nanomaterials, 9 (2019) 1509.
[66] O. Sacco, V. Vaiano, C. Daniel, W. Navarra, V. Venditto, Removal of phenol in aqueous media by N-doped TiO2 based photocatalytic aerogels, Materials Science in Semiconductor Processing, 80 (2018) 104-110.
[67] V. Vaiano, O. Sacco, D. Sannino, Enhanced photocatalytic degradation of organic pollutants in wastewater using photocatalysts coupled with luminescent materials, Chemical Engineering Transactions, 60 (2017) 211-216.
[68] O. Sacco, V. Vaiano, D. Sannino, R. Picca, N. Cioffi, Ag modified ZnS for photocatalytic water pollutants degradation: Influence of metal loading and preparation method, Journal of colloid and interface science, 537 (2019) 671-681.
[69] G. Bagnasco, C. Cammarano, M. Turco, S. Esposito, A. Aronne, P. Pernice, TPR/TPO characterization of cobalt–silicon mixed oxide nanocomposites prepared by sol–gel, Thermochimica acta, 471 (2008) 51-54.
[70] L. Albarano, S. Serafini, M. Toscanesi, M. Trifuoggi, V. Zupo, M. Costantini, D.A. Vignati, M. Guida, G. Libralato, Genotoxicity Set Up in Artemia franciscana Nauplii and Adults Exposed to Phenanthrene, Naphthalene, Fluoranthene, and Benzo (k) fluoranthene, Water, 14 (2022) 1594.
[71] L. Albarano, M. Toscanesi, M. Trifuoggi, M. Guida, G. Lofrano, G. Libralato, In situ microcosm remediation of polyaromatic hydrocarbons: influence and effectiveness of Nano-Zero Valent Iron and activated carbon, Environmental Science and Pollution Research, 30 (2023) 3235-3251.
[72] M. Pansini, G. Dell'Agli, A. Marocco, P.A. Netti, E. Battista, V. Lettera, P. Vergara, P. Allia, B. Bonelli, P. Tiberto, Preparation and characterization of magnetic and porous metal-ceramic nanocomposites from a zeolite precursor and their application for DNA separation, Journal of Biomedical Nanotechnology, 13 (2017) 337-348.
[73] E. Dutková, P. Baláž, P. Pourghahramani, S. Velumani, J. Ascencio, N. Kostova, Properties of mechanochemically synthesized ZnS nanoparticles, Journal of Nanoscience and Nanotechnology, 9 (2009) 6600-6605.
[74] W. Jozwiak, E. Kaczmarek, T. Maniecki, W. Ignaczak, W. Maniukiewicz, Reduction behavior of iron oxides in hydrogen and carbon monoxide atmospheres, Applied Catalysis A: General, 326 (2007) 17-27.
[75] D. Denzler, M. Olschewski, K. Sattler, Luminescence studies of localized gap states in colloidal ZnS nanocrystals, Journal of applied physics, 84 (1998) 2841-2845.
[76] K.N. Devi, T.S. Chanu, L.A. Chanu, W.J. Singh, K.J. Singh, Operational parameters and major active species responsible for the photodegradation of malachite green dye by ZnO/ZnS core–shell nanocomposite photocatalyst, Journal of Materials Research, 38 (2023) 473-483.
[77] S. Horoz, O. Sahin, Investigations of structural, optical, and photovoltaic properties of Fe-alloyed ZnS quantum dots, Journal of Materials Science: Materials in Electronics, 28 (2017) 9559-9565.

[78] S. Kumar, N. Verma, Structural, optical and magnetic investigations on Fe-doped ZnS nanoparticles, Journal of Materials Science: Materials in Electronics, 26 (2015) 2754-2759.
[79] W. He, H. Jia, J. Cai, X. Han, Z. Zheng, W.G. Wamer, J.-J. Yin, Production of reactive oxygen species and electrons from photoexcited ZnO and ZnS nanoparticles: a comparative study for unraveling their distinct photocatalytic activities, The Journal of Physical Chemistry C, 120 (2016) 3187-3195.
[80] L. Isac, A. Enesca, Recent Developments in ZnS-Based Nanostructures Photocatalysts for Wastewater Treatment, International Journal of Molecular Sciences, 23 (2022) 15668.
[81] L.O. Conte, S. Cotillas, A. Sánchez-Yepes, D. Lorenzo, A. Santos, LED visible light assisted photochemical oxidation of HCHs in aqueous phases polluted with DNAPL, Process Safety and Environmental Protection, 168 (2022) 434-442.
[82] S. Khan, X. He, J.A. Khan, H.M. Khan, D.L. Boccelli, D.D. Dionysiou, Kinetics and mechanism of sulfate radical-and hydroxyl radical-induced degradation of highly chlorinated pesticide lindane in UV/peroxymonosulfate system, Chemical engineering journal, 318 (2017) 135-142.
[83] B. Gunawardana, N. Singhal, P. Swedlund, Degradation of chlorinated phenols by zero valent iron and bimetals of iron: a review, Environmental Engineering Research, 16 (2011) 187-203.
[84] C. Daniel, D. Sannino, G. Guerra, Syndiotactic polystyrene aerogels: adsorption in amorphous pores and absorption in crystalline nanocavities, Chemistry of Materials, 20 (2008) 577-582.
[85] A. Mancuso, O. Sacco, V. Venditto, W. Navarra, P. Antico, C. Daniel, V. Vaiano, Selective Absorption of Aromatic Compounds by Syndiotactic Polystyrene Aerogels, in: Macromolecular Symposia, Wiley Online Library, 2023, pp. 2200062.
[86] C. Chang, F. Lian, L. Zhu, Simultaneous adsorption and degradation of γ-HCH by nZVI/Cu bimetallic nanoparticles with activated carbon support, Environmental pollution, 159 (2011) 2507-2514.
[87] Z. Wang, W. Huang, Dechlorination of γ-hexachlorocyclohexane by zero-valent metallic iron, Journal of Hazardous Materials, 166 (2009) 992-997.
[88] N. Radić, B. Grbić, S. Stojadinović, M. Ilić, O. Došen, P. Stefanov, TiO2–CeO2 composite coatings for photocatalytic degradation of chloropesticide and organic dye, Journal of Materials Science: Materials in Electronics, 33 (2022) 5073-5086.